A structural change in $Ca_3Co_4O_9$ associated with enhanced thermoelectric properties

A structural change in Ca₃Co₄O₉ associated with enhanced thermoelectric properties

Tao Wu[1], Trevor A Tyson[1], Haiyan Chen[1], Jianming Bai[2], Hsin Wang[3] and Cherno Jaye[4]

[1] Department of Physics, New Jersey Institute of Technology, Newark, NJ 07102, USA
[2] Materials Science and Engineering, University of Tennessee, Knoxville, TN 37996, USA
[3] Materials Science and Technology Division, Oak Ridge National Laboratory, Oak Ridge, TN 37831, USA
[4] Materials Science and Engineering Laboratory, National Institute of Standards and Technology, Gaithersburg, MD 20899, USA

E-mail: tyson@adm.njit.edu

Abstract
Temperature dependent electrical resistivity, crystal structure and heat capacity measurements reveal a resistivity drop and electrical transport behavior change corresponding to a structural change near 400 K in Ca₃Co₄O₉. The lattice parameter c varies smoothly with increasing temperature while anomalies in a, b_1 and b_2 lattice parameters occur near 400 K. The Ca site in the Ca₂CoO₃ block becomes distorted and a change in electrical transport behavior is found above 400 K. Resistivity and heat capacity measurements as a function of temperature under magnetic field combined with Co L-edge x-ray absorption spectra reveal only a weak spin contribution to this change. Reduced resistivity associated with the structural change enhances the thermoelectric properties at moderately high temperatures and points to the electrical transport behavior change as a mechanism for improved ZT in this thermoelectric oxide.

(Some figures may appear in colour only in the online journal)

1. Introduction

Thermoelectric materials can convert heat to electrical energy directly and vice versa. These materials are of significant importance since they can recycle waste heat (∼70% of the total primary energy in internal combustion systems) and may have significant impact on cooling [1]. The performance of thermoelectric materials is characterized by $ZT = S^2 T \rho^{-1} \kappa^{-1}$, where ZT is a dimensionless figure of merit, S is the Seebeck coefficient, ρ is resistivity and κ is thermal conductivity. The power factor is defined as $P = S^2 \rho^{-1}$, with ZT then given by $PT\kappa^{-1}$. The discovery of NaCo₂O₄ [2], which has a high power factor, generated much interest in a class of oxide-based thermoelectric materials which are environmentally friendly and have high chemical and thermal stability at high temperatures. In this class, the cobaltite [Ca₂CoO₃]₀.₆₂[CoO₂], known as Ca₃Co₄O₉, with incommensurate misfit structure is widely investigated but not well understood. ZT of single crystal Ca₃Co₄O₉ was reported to be ∼1 at 1000 K [3]. Thus it is considered to be a promising p-type thermoelectric material [4]. However, the origin of the high value of ZT at higher temperatures is not understood. Previous investigations explored the structure of various forms (powders, crystals and thin films) and doping dependence and the impact of these properties on the thermoelectric figure of merit etc [5–14]. However, they do not provide a detailed mechanism for the origin of the high ZT values at high temperature.

We note that unlike standard thermoelectrics such as PbTe or Bi₂Te₃, Ca₃Co₄O₉ is a complex incommensurate monoclinic misfit structure (see figure 1) with the superspace group $X2/m(0b0)s0$. It consists of two interpenetrating
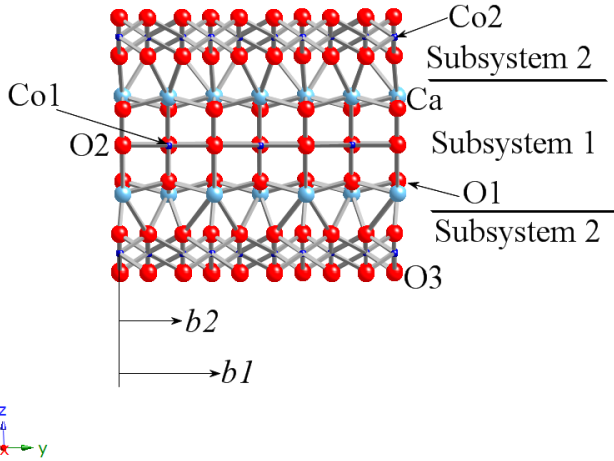
Figure 1. The crystal structure of $Ca_3Co_4O_9$ showing the Ca_2CoO_3 block (subsystem 1) and CoO_2 layer (subsystem 2) with incommensurate b_1 and b_2 axes labeled.

Figure 2. (a) Temperature dependent resistivity and Seebeck coefficient of $Ca_3Co_4O_9$. (b) Temperature dependence of the power factor. The shaded region between 355 and 400 K shows the resistivity anomaly and it is expanded in figure 3.

subsystems of a triple-layered NaCl-type rocksalt Ca_2CoO_3 block (subsystem 1) and a CdI_2-type hexagonal CoO_2 layer (subsystem 2) [5, 9, 15–17]. The subsystems stack along the c axis and share the same a, c and β lattice parameters: $a = 4.8270(5)$ Å, $c = 10.8300(2)$ Å, $\beta = 98.136(1)°$. The mismatch of the unit cells along the b axis results in different b lattice parameters for each subsystem: $b_1 = 4.5615(2)$ Å (subsystem 1) and $b_2 = 2.8173(1)$ Å (subsystem 2) [17]. The CoO_2 layer is conducting and the insulated Ca_2CoO_3 block is regarded as a charge reservoir [18].

The low temperature thermoelectric properties of $Ca_3Co_4O_9$ have attracted much attention both from applications and fundamental science perspectives. It shows metallic electrical conductivity ($\sim$63 Ω^{-1} cm^{-1} at 300 K) while maintaining a high Seebeck coefficient ($\sim$130 μV K^{-1} at 300 K) yielding a high power factor. Two electrical resistivity anomalies have been found (see figure 2(a)), one near 20 K and one around 400 K [15, 19]. The low temperature transition is associated with a change in magnetic order while the anomaly near 400 K has been suggested to be associated with a Co spin state change. Specifically, the abrupt slope change in the inverse magnetic susceptibility (χ^{-1}) around 420 K [15] and the thermal hysteresis loop of χ^{-1} at 380 K [20] was attributed to a spin state transition of cobalt. Moreover, muon spin resonance (μSR) measurements indicated that the Co ions change spin state between intermediate-spin (IS) + low-spin (LS) and intermediate-spin (IS) + high-spin (HS) [21]. Electron energy loss spectroscopy (EELS) suggested that the Co^{3+} ion spin state transition occurs from LS at room temperature to IS at 500 K [22].

In this work, we focus on the region of the resistivity anomaly around 400 K since it impacts the thermoelectric properties at moderately high temperature. The electrical transport behavior change and resistivity drop near 400 K contribute greatly to *ZT* enhancement because the thermal conductivity remains essentially constant and the Seebeck coefficient (figure 2(a)) increases monotonically at moderately high temperatures [3, 23, 24]. Hence it is important to explore
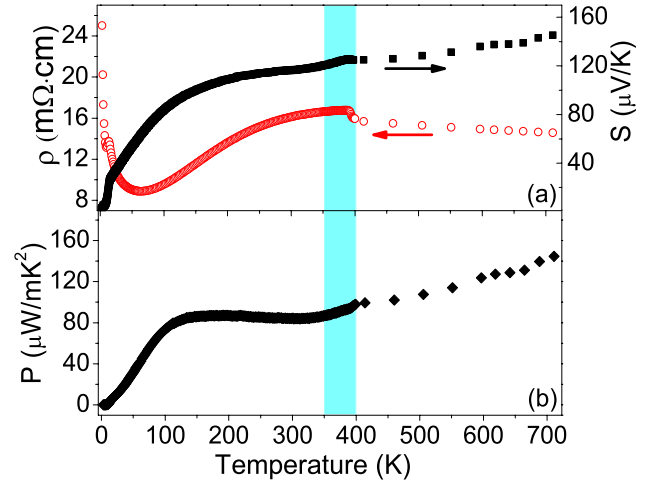
the origin of the changes near 400 K to further improve the thermoelectric properties of $Ca_3Co_4O_9$.

The same series cobaltite, $Na_{0.62}CoO_2$, was found to have a phase transition induced electrical transport behavior change at $\sim$350 K [25]. It is of great importance to investigate whether a structural change induces the resistivity anomaly and to determine the atomic level changes associated with the temperature dependence of the $Ca_3Co_4O_9$ resistivity. A first-order phase transition inducing the electrical transport change of $Ca_3Co_4O_9$ was proposed by differential scanning calorimetry (DSC) measurements [26]. However, no direct structural experiment has been done to substantiate the nature of this structural change. In this work, temperature dependence of resistivity and the Seebeck coefficient of $Ca_3Co_4O_9$ were measured. At the same time, both x-ray diffraction (XRD) and heat capacity measurements as a function of temperature were conducted to explore structural effects on the electrical and thermal transport. We have found that a structural change near 400 K alters the nature of the resistivity curve from one with increasing resistivity with temperature (metal like) to an insulator-like behavior which enhances the power factor. This result gives an example of thermoelectricity enhanced by an electron transport change as a route to a new class of thermoelectric materials.

2. Experimental methods

Single phase polycrystalline $Ca_3Co_4O_9$ was prepared by the solid state reaction. Stoichiometric amounts of high purity $CaCO_3$ and Co_3O_4 were ground, mixed thoroughly and calcined at 900 °C in air for 24 h. The mixture was reground and pressed into a pellet. The pellet was heated at 920 °C in air for 24 h. The latter step was repeated and the final pellet was annealed at 750 °C in flowing oxygen for 36 h. The resistivity, Seebeck coefficient and heat capacity measurements of $Ca_3Co_4O_9$ up to 400 K were carried out with a Physical Property Measurement System (PPMS, Quantum Design)

with magnetic fields up to 8 T. High temperature Seebeck coefficient measurements up to 710 K were conducted on a ZEM-3 at the High Temperature Materials Laboratory (HTML), Oak Ridge National Laboratory. High temperature resistivity was measured by the standard four-probe method up to 710 K in air in a tube furnace using a constant current source and digital voltmeter. *In situ* temperature dependent x-ray diffraction (XRD) measurements between 346 and 438 K were conducted at beamline X14A at the National Synchrotron Light Source (NSLS), Brookhaven National Laboratory (BNL) using a high count rate linear detector. The x-ray wavelength was 0.774 97 Å and the resolution in 2θ was 0.005°. Finely ground $Ca_3Co_4O_9$ powder (<25 μm) was loaded into a glass capillary with an inner diameter of 0.6 mm and was heated by a programmed controlled resistive heating. Rietveld refinement was performed on the XRD data using JANA 2006 [27]. Co L_2-and L_3-edge x-ray absorption spectra were measured in both fluorescence and partial electron yield modes at beamline U7A at NSLS, BNL.

3. Results and discussion

Figure 2(a) shows the temperature dependence of resistivity and the Seebeck coefficient of $Ca_3Co_4O_9$ from 2 K to 710 K. Transport behavior changes at ∼60 K and ∼400 K. The resistivity drops rapidly with increasing temperature below 60 K, indicating insulating behavior. Above this region the system exhibits metal-like transport up to 380 K as the resistivity generally increases with temperature. A sudden drop of resistivity occurs near 400 K and transport behavior changes again (reduced resistivity with increasing temperature) up to 710 K. These electrical transport results on our samples are consistent with the previously published work [15, 19]. The solid black symbols in figure 2(a) show the Seebeck coefficient as a function of temperature. It increases within the whole temperature range and the positive value indicates that holes are the dominant carriers in this system. Figure 2(b) shows the temperature dependent power factor. It increases monotonically within the whole temperature range. The value increases rapidly below 150 K, followed by an almost linear increase. However, a jump is found near 400 K in the shaded window. The enhancement of power factor is attributed to the resistivity change (see below). We focus on both transport and structural changes near 400 K.

In order to see the details of the thermoelectric properties change near 400 K, the temperature dependence of resistivity, the Seebeck coefficient (figure 3(a)) and the power factor (figure 3(b)) from 355 K to 400 K are shown in expanded form. The open and solid circles correspond to the resistivity in warming and cooling cycles, respectively. It increases monotonically with the increasing temperature up to 16.7 mΩ cm at 385 K while the slope (dρ/dT) decreased gradually. Then the magnitude of the resistivity drops at the transition. The same trend can be found in cooling. However, it shifts towards lower temperature by ∼5 K. A hysteresis loop is associated with the resistivity change on warming and cooling processes. The resistivity measurement is reversible. The black diamond symbols give the Seebeck coefficient on
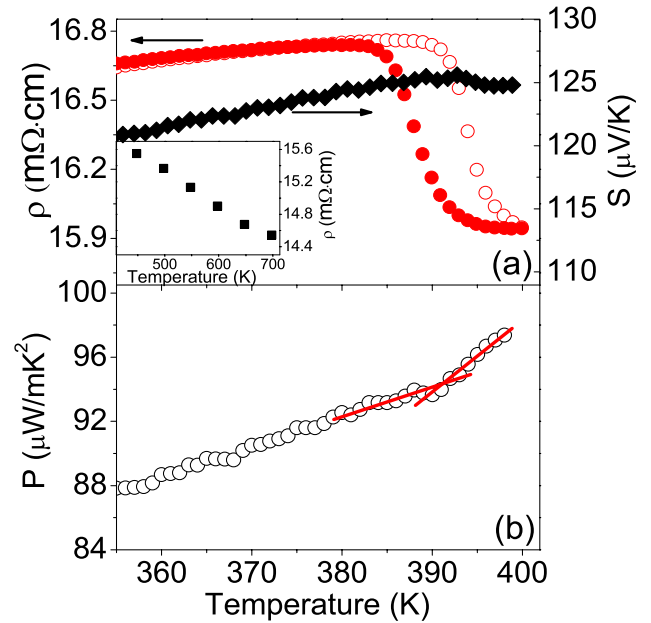

Figure 3. (a) Temperature dependent resistivity and Seebeck coefficient of $Ca_3Co_4O_9$ between 355 K and 400 K. The circle symbols display the resistivity on warming (open circles) and cooling (solid circles) with a hysteresis loop. The Seebeck coefficient is shown on warming. The inset in (a) is the high temperature resistivity showing the insulating transport behavior above 400 K. (b) Temperature dependence of power factor on warming. Note that the resistivity drop results in a significant increase of power factor (slope) near 400 K. The straight lines in (b) are guides to the eye.

warming. It increases with temperature and drops slightly above ∼390 K. The great enhancement of the power factor above 390 K is derived from the resistivity drop (figure 3(b)). Red lines (guides to the eye) give the slope of the power factor as a function of temperature. The inset in figure 3(a) shows the temperature dependence of resistivity at moderately high temperature. It decreases with increasing temperature which indicates the insulating transport behavior.

Results from the Rietveld refinements of synchrotron powder XRD on $Ca_3Co_4O_9$ at 346 K and 438 K are shown in figures 4(a) and (b), respectively. The bump around 10° in 2θ is the background from the glass capillary. Two small unindexed peaks labeled by asterisks (seen also by Grebille *et al* [17]) may originate from an additional modulation vector in the Ca_2CoO_3 block. The superspace group $X2/m(0b0)s0$ was employed in the Rietveld refinement. The observed (crosses), calculated (solid line) and difference (bottom line) profiles in both figures 4(a) and (b) show that both the low and high temperature XRD data are in good agreement with the same model. However, the temperature dependent weighted profile R factor (R_{wp}, see figure 5) shows a sudden increase near 400 K. The average R_{wp} below 400 K is 3.36 ± 0.06% and is 3.63 ± 0.09% above 400 K. This indicates a weak but real deviation from the low temperature structural phase above 400 K. The very subtle structural change and new superspace group will be solved in future neutron powder diffraction measurements. The peak positions (vertical bars) of reflections common to both subsystems (1),
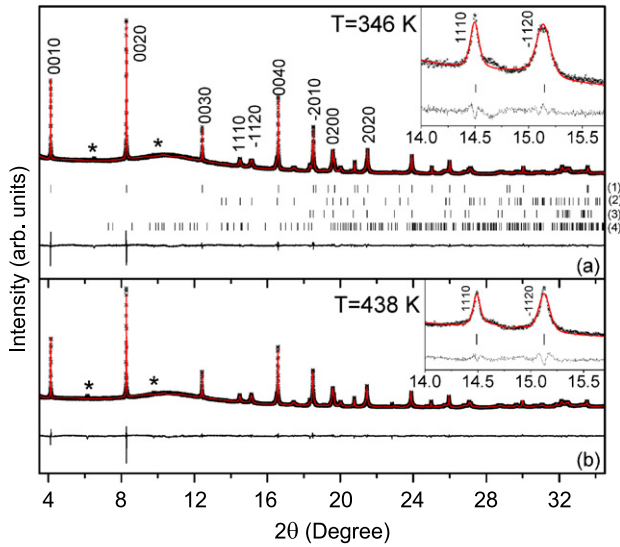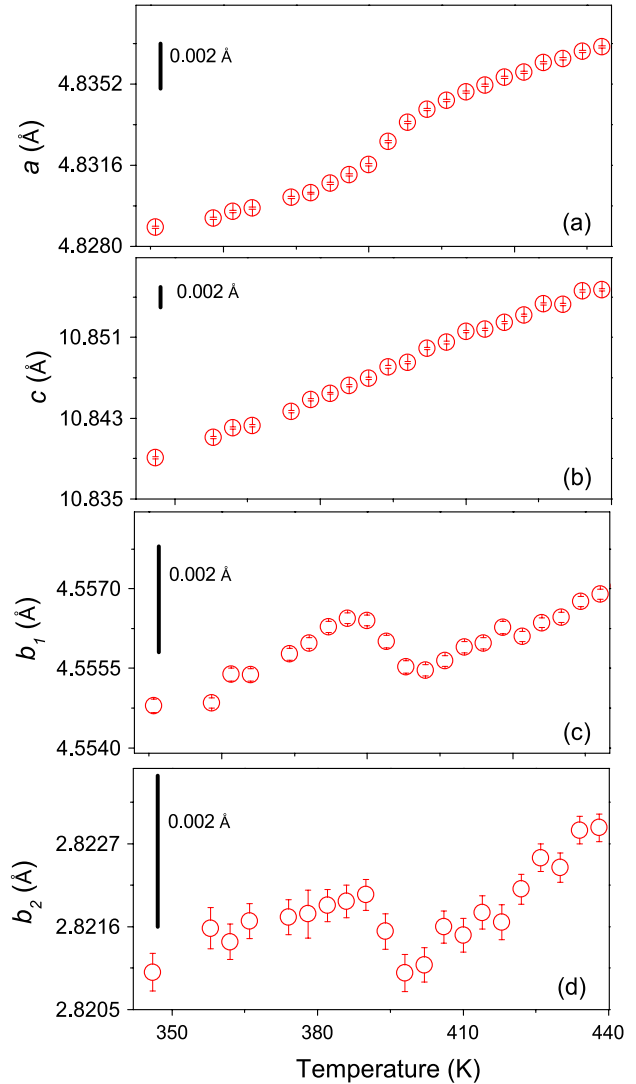
Figure 4. Rietveld refinement of synchrotron powder XRD on
$Ca_3Co_4O_9$ at 346 K (a) and 438 K (b), respectively. The bump
around 10° in 2θ is the background from the glass capillary. Two
weak unindexed peaks (*) are discussed in the text. The observed
(crosses), calculated (solid line) and difference (bottom line)
profiles are shown in both (a) and (b). Peak positions of reflections
common to both subsystems (1), reflections of subsystem 1 (2),
reflections of subsystem 2 (3) and satellite reflections (4) are shown
in (a). The insets in (a) and (b) show the details of the Rietveld
refinement for two specific peaks.
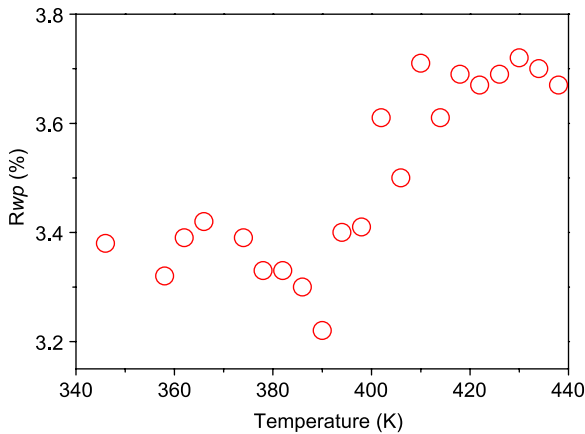
Figure 5. Temperature dependence of the weighted profile R factor
(R_{wp}) of the Rietveld refinements.

Figure 6. Lattice parameters of $Ca_3Co_4O_9$ as a function of
temperature. (a)–(d) correspond to the lattice parameters a, c, b_1 and
b_2 between 346 K and 438 K, respectively. Note that anomalies of
a, b_1 and b_2 are located in the same temperature range as the abrupt
change of resistivity. A vertical bar of height 0.002 Å is included in
each panel to establish a common scale.

reflections of subsystem 1 (2), reflections of subsystem 2 (3)
and satellite reflections (4) are shown in figure 4(a). The
inset in both panels in figure 4 also shows the details of
the Rietveld refinements for specific peaks. The split of the
peak ($\bar{1}120$) was also observed by Grebille *et al*. However,
a lower symmetry structural model cannot improve the
refinements [17]. The split disappears at higher temperatures.
(Figure 1 is the crystal structure of $Ca_3Co_4O_9$. The Ca_2CoO_3
block (subsystem 1) and CoO_2 layer (subsystem 2) with the
mismatched lattice parameters b_1 and b_2 are labeled.)

Figures 6(a)–(d) give the temperature dependence of
lattice parameters a, c, b_1 and b_2 for the temperature range
346 K–438 K on warming, respectively. A vertical bar of

height 0.002 Å is included in each panel to establish a
common scale. Both lattice parameters a and c (figures 6(a)
and (b)) increase monotonically. The slope of a (da/dT)
is steeper in the temperature range 390–400 K while
lattice parameter c increases linearly with the increasing
temperature. The lattice parameter b_1 (figure 6(c)) increases
from 346 to 390 K. Then it drops from 390 to 400 K
followed by an increasing trend. In figure 6(d), parameter
b_2 has the same trend as b_1. It expands with the increasing
temperature, while it drops in the transition temperature
range (390–400 K). b_2 has the biggest error bar compared
to the other lattice parameters since it is obtained by b_1/q
and the error from both b_1 and q was considered. Here q
is a wavevector to describe the mismatch of two different
subsystems and it was obtained directly from Rietveld
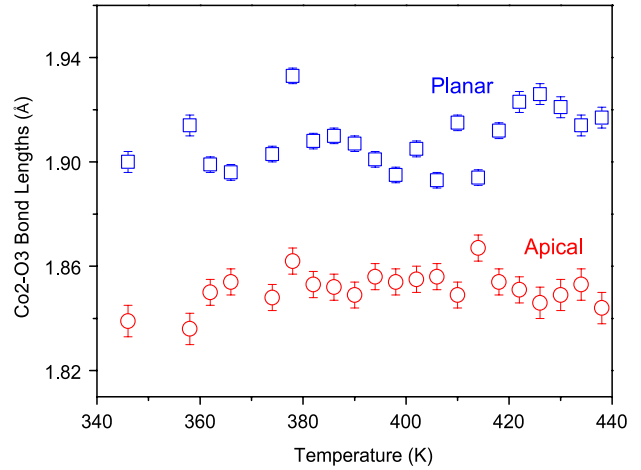refinement. Thus the structure changes in the temperature
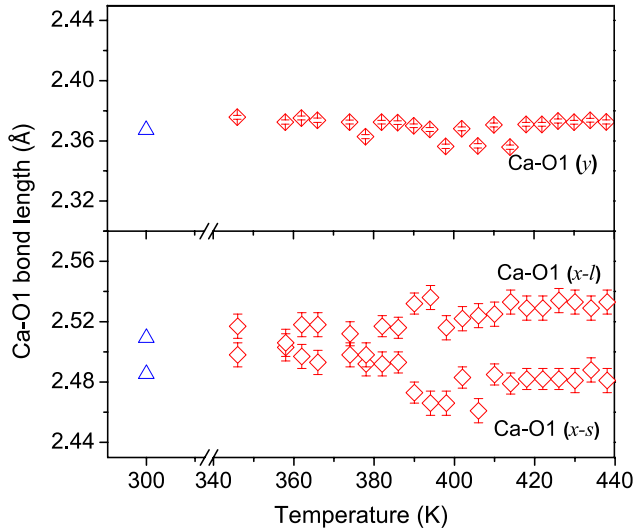
Figure 7. Temperature dependence of Ca–O1 bond lengths in the x–y plane in the Ca₂CoO₃ block. The triangle symbols are the room temperature neutron powder diffraction data from [17]. (a) Ca–O1 (y) shows Ca–O1 bond along y-axis. (b) Ca–O1 (x–l) and Ca–O1 (x–s) are the long and short Ca–O1 bonds along the x-axis, respectively.

Figure 8. Temperature dependent Co2–O3 bond lengths in the CoO₆ octahedron in the conducting CoO₂ layer. The square and circle symbols are planar and apical bonds, respectively. Note that no significant change occurs in the Co2–O3 bonds.

Figure 9. The Co L_2- and L_3-edge spectra of $Ca_3Co_4O_9$ at 380 K (solid line) and 412 K (dash line). Note that the overall shape of the spectra is unchanged.

window 390 –400 K; the change in the x–y plane is dominant. We now explore the atomic level changes involved.

Figure 7 shows the temperature dependent Ca–O1 bonds which are in the x–y plane in the Ca_2CoO_3 block. For comparison, the triangle symbols show the room temperature neutron powder diffraction data from [17]. It is consistent with the Ca–O1 bonds from this work. Ca–O1 (y) along the y-axis does not change significantly within the whole temperature range. Ca–O1 (x–s) and Ca–O1 (x–l) bonds have a difference ∼0.02 Å below the structural change. However, the separation suddenly increases by ∼0.05 Å above 390 K. This indicates that Ca atoms move to off center positions between neighboring oxygen atoms above 390 K. Thus this layer becomes more distorted possibly due to charge localization associated with the structure change, as seen in the charge ordered phase of the classical manganites.

Figure 8 shows the temperature dependent Co2–O3 bond lengths in the CoO₆ octahedron in the conducting CoO₂ layer. The square and circle symbols are planar and apical bonds. The Co2–O3 bond lengths in this work are in the window of 1.85–1.95 Å which is consistent with the data published by Grebille *et al* [17]. No significant change of the Co2–O3 bonds occurs within the whole temperature range. In addition, the Co L_2-and L_3-edge x-ray absorption spectrum in figure 9 gives the same result. The solid and dashed lines show the data at 380 K and 412 K which are below and above the resistivity anomaly temperature. The unchanged overall shape of the spectra indicates that the local structure and valence around the Co atom does not change significantly during the structural change near 400 K. No significant distortions about the Co sites manifested as change in line shapes due to loss or gain of final state (d band) degeneracy.

The resistivity and structural parameters all display abrupt changes near 400 K. The drop of the resistivity
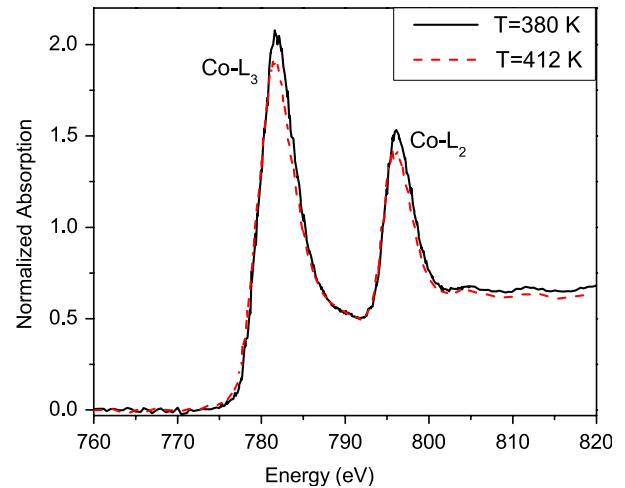
at ∼390 K is connected with the discontinuity of the lattice parameters a, b_1 and b_2 as well as the distortion in the Ca_2CoO_3 block. The stability of the CoO_2 layer in the whole temperature range indicates that the Ca_2CoO_3 block dominates the structural change. The resistivity drop might result from a carrier increase since the Ca_2CoO_3 block is considered as a charge reservoir. The out-of-plane lattice parameter c changes linearly with temperature. It can be understood in terms of dominant in-plane conduction/resistivity of $Ca_3Co_4O_9$ observed by Masset *et al* [15].

Besides the structural effects, the spin contribution to the change near 400 K was also investigated. Specifically, resistivity and heat capacity measurements as a function of magnetic field were performed. Figure 10(a) gives the temperature dependent resistivity of $Ca_3Co_4O_9$ within the temperature region 355–400 K in magnetic fields from 0 T
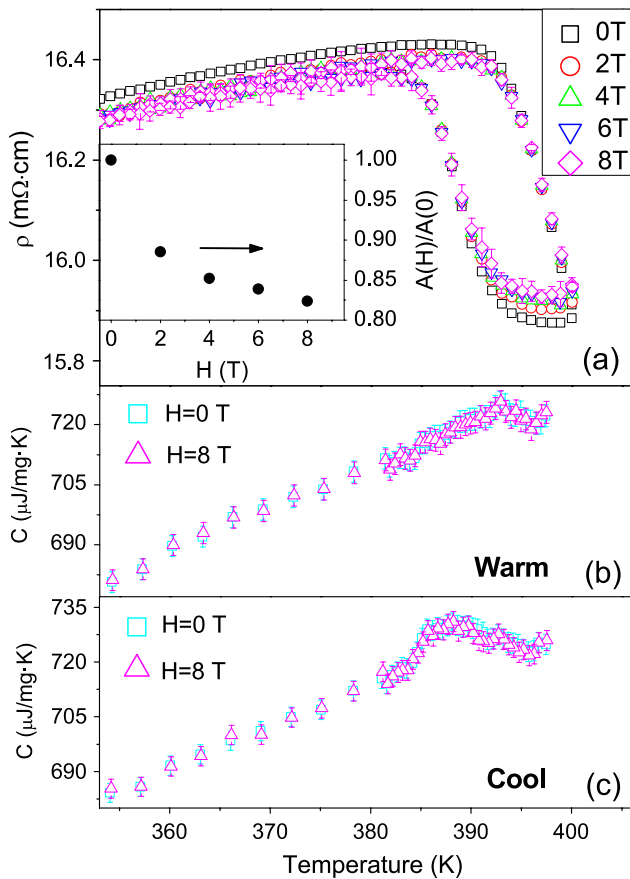
Figure 10. (a) Hysteresis loop of resistivity for magnetic fields up to 8 T. The inset shows the relative area of the hysteresis loop as a function of magnetic field. Temperature dependent heat capacity with $H = 0$ T and 8 T for warming (b) and cooling (c) processes, respectively.

to 8 T with a step size of 2 T. The shape of the hysteresis loop does not change with increasing magnetic fields. However, the area of the hysteresis loop shrinks with the increasing magnetic field. The data set with the largest error bars has these errors included and it indicates that the resistivity change with magnetic fields is real but small. The area of the hysteresis loop in each magnetic field was calculated to obtain the quantitative area change. The *inset* in figure 10(a) shows the relative area change of the hysteresis loop ($A(H)/A(0)$). Here $A(H)$ is the hysteresis loop area in the magnetic field H and $A(0)$ is the area without magnetic field. The area reduces rapidly at low magnetic field and then shrinks gradually up to 8 T. The magnetic field dependence of the hysteresis loop indicates there is a spin contribution to the electrical transport (or that the spin and lattice are coupled). Figures 10(b) and (c) are the temperature dependent heat capacity with magnetic field in warming and cooling cycles, respectively. The square symbols are for zero field and the triangle symbols are at 8 T. The zero field and 8 T data overlap completely in the whole temperature range on both warming and cooling. Within the statistical errors, the heat capacity does not change with the magnetic field. Thus there is no evidence of spin ordering contribution from the heat capacity measurements. In addition since a significant part of the heat capacity is derived from

the phonons' spectrum it also suggests that the spin–lattice coupling is weak. Moreover, the unchanged shape of Co L_2-and L_3-edge x-ray absorption spectra at 380 K and 412 K (figure 9) reveals no change in the average Co spin state. In terms of the magnitude of spins on the Co sites, it is possible that only a small fraction of Co ions change spin. Electrical transport is sensitive to even small spin state changes since the electrons take paths of lowest resistance. The change may be below the level of detectability of our heat capacity and x-ray absorption spectroscopy measurements.

4. Summary

In summary, temperature dependent resistivity measurements on $Ca_3Co_4O_9$ reveal a resistivity anomaly near ~400 K. XRD measurements as a function of temperature directly reveal a structural change and indicate the associated atomic level changes. The spin contribution to this change was investigated by resistivity and heat capacity measurements under magnetic field and Co L-edge x-ray absorption spectroscopy measurements. The hysteresis loops of resistivity shrink with increasing magnetic field. However, no Co spin state change was found from the heat capacity and x-ray absorption measurements. It can be understood that only a small spin state change occurs locally near 400 K. The results give an example of thermoelectricity enhanced by an electrical transport change and point to a new approach for creating materials with high *ZT* values at moderately high temperature in complex oxide systems.

References

[1] Tritt T M and Subramanian M A 2006 *MRS Bull.* **31** 188–98
[2] Terasaki I, Sasago Y and Uchinokura K 1997 *Phys. Rev.* B **56** R12685
[3] Shikano M and Funahashi R 2003 *Appl. Phys. Lett.* **82** 1851–3
[4] Ohta H, Sugiura K and Koumoto K 2008 *Inorg. Chem.* **47** 8429–36
[5] Miyazaki Y, Onoda M, Oku T, Kikuchi M, Ishii Y, Ono Y, Morii Y and Kajitani T 2002 *J. Phys. Soc. Japan* **71** 491–7
[6] Liu Y H, Lin Y H, Jiang L, Nan C W and Shen Z J 2008 *J. Electroceram.* **21** 748–51

[7] Wang Y, Sui Y, Cheng J, Wang X, Su W, Liu X and Fan H J 2010 *J. Phys. Chem.* C **114** 5174–81

[8] Wang Y, Sui Y, Ren P, Wang L, Wang X, Su W and Fan H 2010 *Chem. Mater.* **22** 1155–63

[9] Muguerra H, Grebille D and Bourée F 2008 *Acta Crystallogr.* B **64** 144–53

[10] An M, Yuan S K, Wu Y, Zhang Q M, Luo X G and Chen X H 2007 *Phys. Rev.* B **76** 024305

[11] Eng H W, Limelette P, Prellier W, Simon C and Fresard R 2006 *Phys. Rev.* B **73** 033403

[12] Masuda Y, Nagahama D, Itahara H, Tani T, Seo W S and Koumoto K 2003 *J. Mater. Chem.* **13** 1094–9

[13] Pei J, Chen G, Lu D Q, Liu P S and Zhou N 2008 *Solid State Commun.* **146** 283–6

[14] Zhao B C, Sun Y P, Lu W J, Zhu X B and Song W H 2006 *Phys. Rev.* B **74** 144417

[15] Masset A C, Michel C, Maignan A, Hervieu M, Toulemonde O, Studer F, Raveau B and Hejtmanek J 2000 *Phys. Rev.* B **62** 166–75

[16] Lambert S, Leligny H and Grebille D 2001 *J. Solid State Chem.* **160** 322–31

[17] Grebille D, Lambert S, Bourée F and Petrícek V 2004 *J. Appl. Crystallogr.* **37** 823–31

[18] Li Q 2006 *Mater. Res. Soc. Symp. Proc.* **886** 0886-F01-05

[19] Miyazaki Y, Kudo K, Akoshima M, Ono Y, Koike Y and Kajitani T 2000 *Japan. J. Appl. Phys. 2* **39** L531–3

[20] Sugiyama J, Xia C T and Tani T 2003 *Phys. Rev.* B **67** 104410

[21] Sugiyama J, Brewer J H, Ansaldo E J, Itahara H, Bayer M and Tani T 2003 *Physica* B **326** 518

[22] Yang G, Ramasse Q and Klie R F 2009 *Appl. Phys. Lett.* **94** 093112

[23] Xu G J, Funahashi R, Shikano M, Matsubara I and Zhou Y Q 2002 *Appl. Phys. Lett.* **80** 3760–2

[24] Wang Y, Sui Y, Cheng J G, Wang X J, Su W H and Fan H J 2010 *Appl. Phys.* A **99** 451–8

[25] Blangero M, Carlier D, Pollet M, Darriet J, Delmas C and Doumerc J-P 2008 *Phys. Rev.* B **77** 184116

[26] Cheng J, Sui Y, Wang Y, Wang X and Su W 2009 *Appl. Phys.* A **94** 911–6

[27] Petricek V, Dusek M and Palatinus L 2006 *The Crystallographic Computing System* (Prague: Institute of Physics)